Distribution of marine ice beneath the Amery Ice Shelf

Helen Amanda Fricker[1]

Sergey Popov[2]

Ian Allison[3] and Neal Young[3]

Abstract. We present a map of the marine ice accreted to the base of the Amery Ice Shelf (AIS), East Antarctica. This map is obtained by converting a Digital Elevation Model (DEM) of the AIS generated from satellite radar altimeter data to an ice thickness map, assuming hydrostatic equilibrium, and subtracting from that a second ice thickness map, derived from airborne radio-echo sounding (RES) measurements. The RES signal does not penetrate the marine ice, so the measurement is only to the meteoric-marine ice boundary, and therefore the difference between the two maps is the marine ice thickness. The marine ice is up to 190 m thick and accounts for about 9% of the shelf volume. It is concentrated in the northwest of the shelf, a result of the clockwise ocean circulation in the cavity below.

Introduction

A significant fraction of the ice flowing from the interior of the Antarctic ice sheet is lost by melting under the deeper parts of ice shelves [*Jacobs et al.*, 1992]. This melt cools and freshens seawater circulating in the sub-ice-shelf cavity, and can lead to accretion of "marine" ice elsewhere under the shelf [*Jenkins and Doake*, 1991]. Net meltwater production (basal melting minus freezing) is critical for both mass balance of the ice sheet, and for the freshwater flux to the Southern Ocean. Meltwater may also mix with warmer, saltier Circumpolar Deep Water on the continental slope and contribute to Antarctic Bottom Water production [*Wong et al.*, 1998]. Water properties in the inaccessible sub-ice-shelf cavities are difficult to measure. The rate and distribution of basal freezing is sensitive to the melt rate, and to the properties and circulation of water in the cavity, and hence provide indirect information on these parameters. Here we show the distribution of marine ice beneath the Amery Ice Shelf (AIS; Fig. 1), one of the major embayed ice shelves of Antarctica.

Method

For a freely floating ice shelf, the relationship between the surface height H (relative to sea level) and the thickness Z at any point is given by the hydrostatic equation:

$$H = \frac{Z(\rho_w - \rho_i)}{\rho_w} \quad (1)$$

where ρ_w and ρ_i are the column-averaged densities of seawater and ice respectively. We define the hydrostatic height anomaly $(\delta h')$ as the difference between the measured surface height and the surface height calculated from measured ice thickness using Equation 1. $\delta h'$ will be significant for grounded ice (where Equation 1 does not hold), or where there are errors in the total thickness or density values. Errors in measurement of the total ice thickness using RES systems can occur where a marine ice layer is present [*Thyssen*, 1988]. RES systems typically detect the meteoric-marine ice boundary, since it exhibits a moderate dielectric contrast but the signal may not penetrate the marine ice layer itself because of high absorption of electromagnetic energy within [*Blindow*, 1994]. $\delta h'$ can thus be used to provide an estimate of the thickness and extent of marine ice that underlies ice masses that are known to be floating.

Data

We applied Equation 1 to the AIS using data collected by satellite and aircraft. We used surface heights from a DEM of the AIS (AIS–DEM) generated from ERS-1 satellite radar altimetry [*Fricker et al.*, 2000] combined with geoid-ellipsoid separation values from the Earth Gravitational Model 1996 (EGM96) [*Lemoine et al.*, 1998]. We used airborne RES ice thickness measurements made by the Russia PMGRE (Fig. 2). The column-averaged density of the seawater displaced by the ice shelf was taken as 1029 kg m^{-3}, derived from measurements made off the front [*Wong et al.*, 1998].

Column-averaged ice density was taken from a two-layer density model for the meteoric ice (Table 1), with an upper layer 100 m thick, and the X-axis oriented approximately along the ice flow direction. Most of the spatial variability in the column-averaged density results from near-surface variations associated with the surface mass budget. Between X=0 and 300 the surface is mainly an ablation zone or covered by superimposed ice. North of X=300, snow accumulation is positive and increases towards the front. Here a firn layer develops which attains an approximately equilibrium thickness of 30 m around X=400. The density of the lower layer, from 100 m to the base, is determined essentially by temperature [*Pounder*, 1965]. The mean column temperature within this layer, derived from numerical modelling, varies linearly in the flow direction from –30°C at the southern end to –10°C at the 1968 G1 borehole site (69.451°S, 71.497°E) [*Budd et al.*, 1982]. Snow accumulation rates also vary mainly in the flow direction [*Budd*, 1966]

---

[1] IGPP, Scripps Institution of Oceanography, University of California San Diego, La Jolla

[2] Polar Marine Geological Research Expedition (PMGRE), St. Petersburg, Russia

[3] Antarctic CRC & Australian Antarctic Division, Hobart, Tasmania, Australia

so we assume that mean densities within the two meteoric ice layers vary only in the X-direction. Specular RES bottom echoes indicate that melting occurs under much of a flow-band on the eastern side of the shelf, originating from the Lambert Glacier. Other observations show that the ice is floating here [*Fricker et al.*, in revision] and we are therefore confident that the RES has measured the total thickness. The variation of column-averaged-density with distance along this band, estimated using Equation 1, is used to set the model change points (Table 1) and to constrain the upper layer model parameters. Densities along here exhibit variability consistent with the surface conditions described above. Where marine ice is found we introduce a third layer with a density of 917 kg m^{-3}.

Results

The hydrostatic condition is satisfied over most of the ice shelf as far south as 73.2°S near Mawson Escarpment (Fig. 3a). There are two regions where $\delta h'$ is significant: i) over grounded ice where Equation 1 does not apply, thus delineating the fl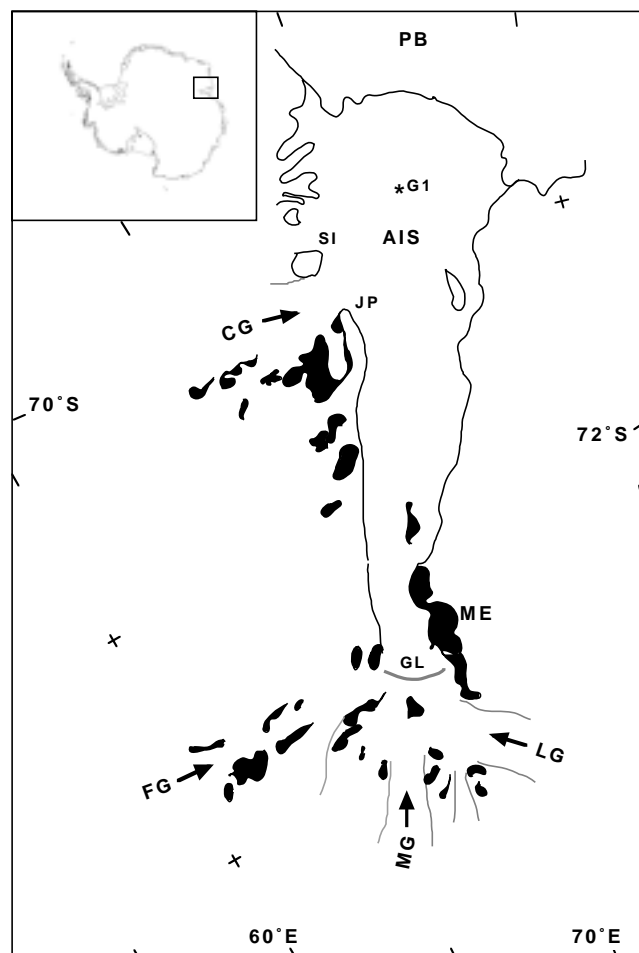oating portion of the AIS-Lambert Glacier system [*Fricker et al.*, in revision] and ii) in the northwestern part of the ice shelf where $\delta h'$ is up to +26 m. We attribute this anomaly to a marine ice layer accreted to the ice shelf base, which causes an error in the ice thickness measurement.

We estimated the thickness of the marine ice layer (Fig. 3b) by subtracting the RES ice thickness map from a second ice thickness map calculated from the surface height data (AIS–DEM plus EGM96) using Equation 1 and the density model. Since the RES technique only measures to the top of the marine ice layer, the difference between these two maps gives the thickness of the marine ice. Under the northwestern part of the shelf the marine ice is up to 190 m thick, contributing
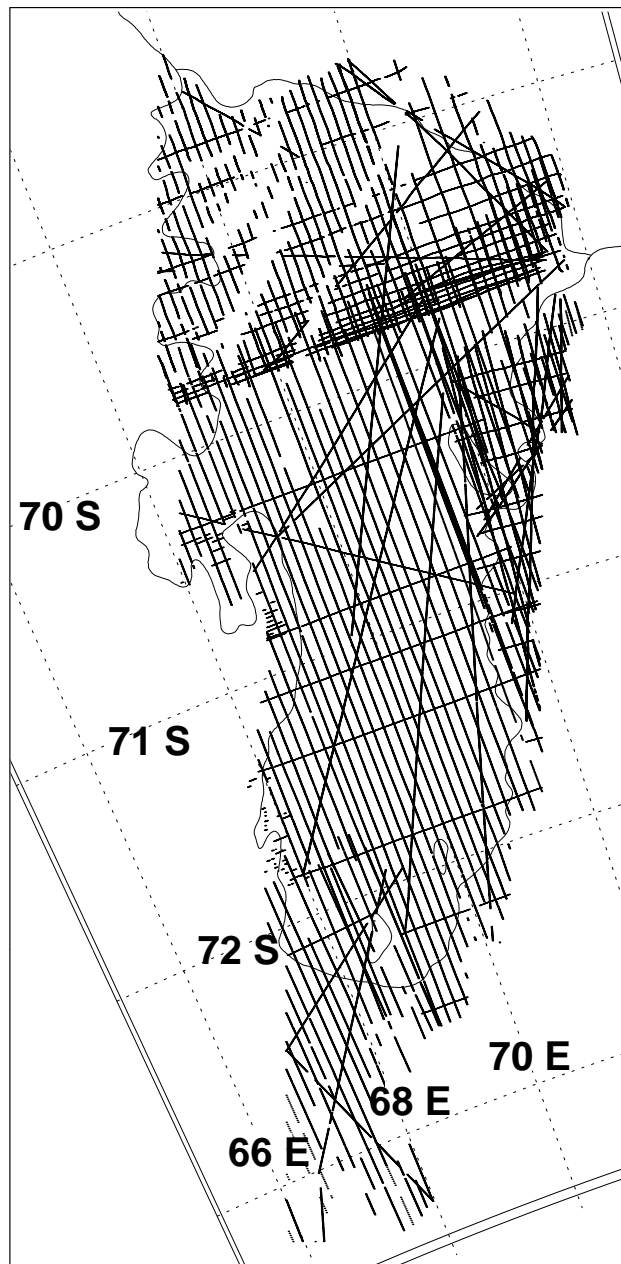

Figure 1. Location map of the AIS, with major ice inflows indicated by solid arrows and key features annotated. AIS: Amery Ice Shelf; PB: Prydz Bay, CG: Charybdis/Scylla glaciers; FG: Fisher Glacier; LG: Lambert Glacier; MG: Mellor Glacier; JP: Jetty Peninsula; ME: Mawson Escarpment; SI: Single Island; G1: 1968 borehole site; GL: newly defined grounding line of *Fricker at al.*, [in revision].

Figure 2. Distribution of Russian PMGRE airborne RES measurements over the AIS, collected during 7 field seasons between 1986 and 1995. Data were interpolated onto the same grid as the AIS–DEM using kriging.

Table 1. Column-averaged densities of the upper (0 to 100 m) and lower (100 m to base of meteoric ice) layers at the change points of the two-layer density model for the AIS.

X (m)[a]	ρ_{upper} (kg m^{-3})	ρ_{lower} (kg m^{-3})
0	910	922
300	905	916
400	800	913
600	785	912

X=0 is just south of the AIS grounding zone. Values are linearly interpolated between these change points.

9% of the total volume of the AIS.

There are several sources of error in our estimate of marine ice thickness. The EGM96 geoid model, used to convert from ellipsoidal to orthometric height, is not reliable in Antarctica due to the paucity of gravity measurements. Geoid errors may be up to 1-2 m over the northern part of the ice shelf and 3-4 m in the south where there is major geological relief. Combined with the RMS error of 1.7 m in the AIS–DEM heights [*Fricker et al.*, 2000], this could lead to an error of around 2-5 m in the orthometric height value. Errors in RES data arise from uncertainty in the speed of radio waves in ice and firn, navigation errors, and limitations digitising RES film records [*Vaughan et al.*, 1995]. The RMS of ice thickness differences at intersections of RES flight lines in the northwest part of the shelf is 26 m. There are also uncertainties in our density model for the ice shelf. Combining all errors our estimated marine ice layer thickness has an uncertainty of about 30 m. In 1968 an ice core was taken from the top 315 m of the ice shelf near G1 (Fig. 3b) [*Morgan*, 1972]. The depth of the meteoric-marine ice boundary was detected in this core with conductivity and $^{18}O/^{16}O$ isotope measurements, and the thickness of the marine layer was inferred as 158 m. Our estimation of the marine ice thickness at this location is 141 m $\pm$ 30 m, consistent with the *Morgan* [1972] estimate.

Discussion

RES records show strong basal echoes under the eastern side (south of 71.3°S) and under the southern ice shelf, from which we infer basal melting. The implied distribution of melting and freezing results from a three-dimensional ocean circulation under the AIS that is clockwise in the x-y plane, combined with a vertical (y-z plane) sub-ice-shelf thermohaline component [*Jenkins and Bombosch*, 1995]. High Salinity Shelf Water (HSSW), formed during winter sea-ice production in Prydz Bay, sinks to the ocean floor and flows under the eastern side of the ice shelf. Depression of the freezing point with increasing pressure [*Lewis and Perkin*, 1986] enables HSSW to cause melting when it comes into contact with the deep ice shelf base. Colder, fresher Ice Shelf Water (ISW) modified by melting circulates clockwise and rises along the gradient of the ice shelf draft, on the west side. At a critical depth the freezing point becomes less than the physical temperature, the ISW is now supercooled, and platelet ice crystals form and accrete (as marine ice) onto the base of the shelf. Fresh, supercooled water plumes containing platelet crystals have been observed north of the ice shelf front in western Prydz Bay [*Penrose et al.*, 1994]. The changes in temperature and salinity characteristics between
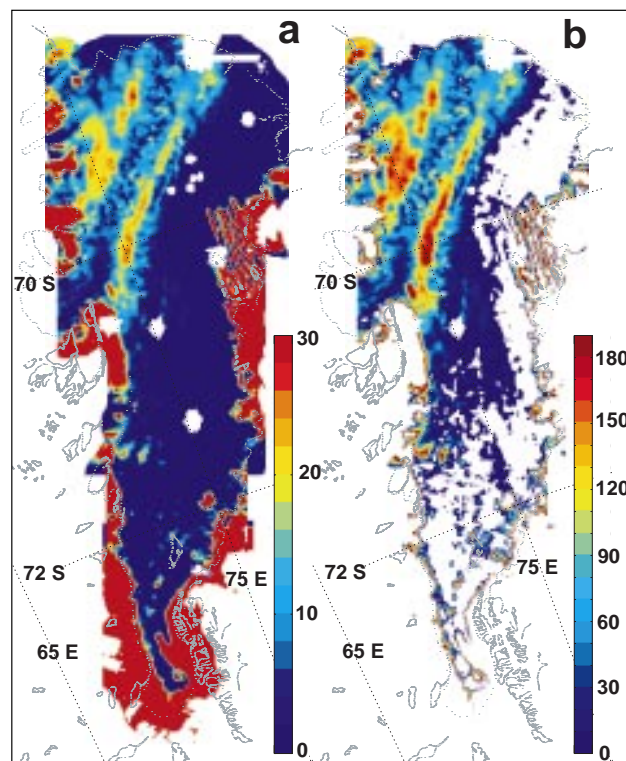

Figure 3. Distribution of a) hydrostatic height anomaly ($\delta h'$) and b) thickness of marine computed for the AIS. Grey lines are a base map of the region (coastline, AIS margin with 1997 ice front, and rock outcrops). White areas in $\delta h'$ plot correspond to null values in the RES map resulting from kriging.

the water entering and exiting the cavity give an estimate of net meltwater production of between 11 and 22 Gt a^{-1} [*Wong et al.*, 1998], which is a substantial fraction of the total continental ice which discharges into the AIS. The influx of ice into the southern AIS from the Lambert, Mellor, Fisher and other tributary glaciers (Fig. 1) is 31 Gt a^{-1} [*Fricker et al.*, in revision] although there are other inputs from ice streams entering the sides of the AIS further north. The marine ice distribution in Fig. 3b is consistent with accretion zones obtained from modelling the three-dimensional ocean circulation beneath the AIS [*Williams et al.*, 1998], and subsequent ice shelf flow.

The thickest marine ice occurs in two longitudinal bands, oriented along the ice flow direction. These are located each side of the Charybdis/Scylla glacier inflow where this stream merges with the AIS downstream of Jetty Peninsula, and with an unnamed stream from north of Single Island. Marine ice preferentially accretes in troughs formed under thinner ice at the margins of these streams. This pattern of marine ice accretion is comparable to that occurring under the Ronne Ice Shelf downstream of peninsulas and ice rumples [*Thyssen et al.*, 1993; *Blindow*, 1994]. The maximum AIS marine ice thickness is 190 m, compared to 140 m for the Filchner Ice Shelf [*Grosfeld*, 1998] and 350 m for the Ronne [*Thyssen et al.*, 1993]. However, the estimated thickness of marine ice under the Ross Ice Shelf is less than 10 m [*Neal*, 1979]. This variation between ice shelves is most likely due to a combination of the different cavity geometries, especially the ice shelf drafts, and the different water properties

and circulation. The AIS has a long, narrow, sub-ice-shelf cavity with a maximum draft of about 2200 m. The Filchner and Ronne ice shelves also have deep drafts (about 1400 m), whereas the Ross Ice Shelf has a shallower draft (about 800 m) and a smaller length-to-width ratio. A major contrast between the AIS marine ice pattern and that under other ice shelves is that it persists all the way to the ice front, and therefore is still present when icebergs calve. Under the Filchner and Ronne ice shelves, a warm subshelf current melts the marine ice layer before it reaches the calving front [*Thyssen et al.*, 1993]. Green icebergs from the AIS, which have capsized since calving thus revealing the marine ice, have been observed in Prydz Bay and further west [*Warren et al.*, 1993].

Basal melting and freezing are significant components of the mass budget of the AIS. Although the effect of future climate warming on these processes is unknown, it is expected that their rate and distribution will change with any warming-induced perturbation to the present sub-ice-shelf thermohaline circulation [*Williams et al.*, 1998]. The marine ice distribution we present here provides a constraint for numerical models of processes occurring within the cavity, which will in turn provide improved estimates of the net melt rate. Continued monitoring of AIS marine ice thickness will not only provide an indicator of change in the ocean conditions, but may also provide early signs of major structural change in the ice shelf itself.

References

Blindow, N., The central part of the Filchner-Ronne Ice Shelf, Antarctica: internal structures revealed by 40 MHz monopulse RES. *Ann. Glaciol.*, *20*, 365–371, 1994.

Budd, W., The Dynamics of the Amery Ice Shelf. *J. Glaciol.*, *6*, 45, 335–358, 1966.

Budd, W. F, M. J. Corry, and T. H. Jacka, Results from the Amery Ice Shelf project. *Ann. Glaciol.*, *3*, 36–41, 1982.

Fricker, H. A., G. Hyland, R. Coleman, and N. W. Young, Models for the Lambert Glacier-Amery Ice Shelf system, East Antarctica, from ERS-1 satellite radar altimetry, *J. Glaciol.*, *46*, 155, 553–560, 2000.

Fricker, H. A., I. Allison, M. Craven, G. Hyland, A. Ruddell, N. W. Young, R. Coleman, M. King, K. Krebs, S. Popov, Redefinition of the grounding zone of the Amery Ice Shelf, East Antarctica, *J. Geophys. Res.*, in revision.

Grosfeld, K., H. H. Helmer, M. Jonas, H. Sandhager, M. Schulte, and D.G. Vaughan, Marine ice beneath Flichner Ice Shelf from a multi-disciplinary approach, in *Ocean, Ice, and Atmosphere: Interactions at the Antarctic Continental Margin*, edited by S. S. Jacobs and R. F. Weiss, Ant. Res. Series, AGU, 75, 319–339, 1998.

Jacobs, S. S., H.H Helmer, C. S. M. Doake, A. Jenkins, and R. M. Frolich, Melting of the ice shelves and the mass balance of Antarctica, *J. Glaciol.*, *38*, 130, 375–387, 1992.

Jenkins, A. and C. S. M. Doake, Ice-Ocean Interaction on Ronne Ice Shelf, Antarctica, *J. Geophys. Res.*, *96*, C1, 791–813, 1991.

Jenkins, A. and A. Bombosch, Modeling the effects of frazil ice crystals on the dynamics and thermodynamics of Ice Shelf Water plumes, *J. Geophys. Res.*, *100*, C4, 6967–6981, 1995.

Lemoine, F. G., S. C. Kenyon, J. K. Factor, R. G. Trimmer, N. K. Pavlis, D. S. Chinn, C. M. Cox, S. M. Klosko, S. B. Luthcke, M. H. Torrence, Y. M. Wang, R. G. Williamson, E. C. Pavlis, R. H. Rapp and T. R. Olson, The development of the joint NASA GSFC and NIMA geopotential model EGM96, *NASA/TP-1998-206861*, National Aeronautics and Space Administration, Goddard Space Flight Center, Greenbelt, MD, 1998.

Lewis, E. L. and R. G. Perkin, Ice pumps and their rates, *J. Geophys. Res.*, *91*, 11,756–11,762, 1986.

Morgan, V. I. Oxygen isotope evidence for bottom freezing on the Amery Ice Shelf. *Nature*, *238*, 393–394, 1972.

Neal, C. S., The dynamics of the Ross Ice Shelf revealed by radio echo-sounding. *J. Glaciol.*, *24*, 90, 295–307, 1979.

Penrose, J., M. Conde and T. Pauly, Acoustic detection of ice crystals in Antarctic waters, *J. Geophys. Res.*, *99*, C6, 12,573–12,580, 1994.

Pounder, E. R. *The Physics of Ice* 151 pp., Pergamon Press, London, 1965.

Thyssen, F., Special aspects of the central part of Filchner-Ronne Ice Shelf, *Ann. Glaciol.*, *11*, 173–179, 1988.

Thyssen, F., A. Bombosch and H. Sandhager, Elevation, ice thickness and structure mark maps of the central part of the Filchner-Ronne Ice Shelf, *Polarforschung.*, *62*, 1, 17–26, 1993.

Vaughan, D. G., J. Sievers, C. S. M. Doake, H. Hinze, D. R. Mantripp, V. S. Pozdeev, H. Sandhager, H. W. Schenke, A. Solheim and F. Thyssen, Subglacial and Seabed Topography, Ice Thickness and Water Column Thickness in the vicinity of Filchner-Ronne-Schelfeis, Antarctica, *Polarforschung.*, *64*, 2, 75–88, 1993.

Warren, S. G., C. S. Roesler, V. I. Morgan, R. E. Brandt, I.D. Goodwin and I. Allison, Green icebergs formed by freezing of organic-rich seawater to the base of Antarctic ice shelves, *J. Geophys. Res.*, *98*, C4, 6921–6928, 1993.

Williams, M. J. M., R. C. Warner and W. F. Budd, The effects of ocean warming and ocean circulation under the Amery Ice Shelf, East Antarctica, *Ann. Glaciol.*, *27*, 75–80, 1998.

Wong, A. P. S., N. L. Bindoff and A. Forbes, Ocean ice-shelf interaction and possible bottom water formation in Prydz Bay, in *Ocean, Ice, and Atmosphere: Interactions at the Antarctic Continental Margin,* edited by S. S. Jacobs and R. F. Weiss, Ant. Res. Series, AGU, 75, 173–187, 1998.

Helen Amanda Fricker (née Phillips), IGPP, Scripps Institution of Oceanography, University of California San Diego, La Jolla, CA 92093-0225. email:hafricker@ucsd.edu

Sergey Popov, PMGRE, Pobeda str. 24, St. Petersburg, Lomonosov 189 510, Russia

Ian Allison and Neal W. Young, Antarctic CRC & Australian Antarctic Division, GP0 Box 252-80, Hobart, TAS 7001, Australia